Subject-specific model-derived kinematics of the shoulder based on skin markers during arm abduction up to 180° - assessment of 4 gleno-humeral joint models

Raphaël Dumas, Sonia Duprey

Journal Pre-proofs

Short communication

Subject-specific model-derived kinematics of the shoulder based on skin markers during arm abduction up to 180° - Assessment of 4 gleno-humeral joint models

R. Dumas, S. Duprey

PII: S0021-9290(22)00115-4
DOI: https://doi.org/10.1016/j.jbiomech.2022.111061
Reference: BM 111061

To appear in: *Journal of Biomechanics*

Received Date: 7 September 2021
Revised Date: 1 February 2022
Accepted Date: 21 March 2022

Please cite this article as: R. Dumas, S. Duprey, Subject-specific model-derived kinematics of the shoulder based on skin markers during arm abduction up to 180° - Assessment of 4 gleno-humeral joint models, *Journal of Biomechanics* (2022), doi: https://doi.org/10.1016/j.jbiomech.2022.111061

Subject-specific model-derived kinematics of the shoulder based on skin markers during arm abduction up to 180° - Assessment of 4 gleno-humeral joint models

Dumas, R., Duprey, S.*

Univ Lyon, Université Claude Bernard Lyon 1, Univ Gustave Eiffel, IFSTTAR, LBMC UMR_T9406, F69622, Lyon, France

*Corresponding author: Sonia DUPREY, PhD, sonia.duprey@univ-lyon1.fr
LBMC, Univ Eiffel – Cité des Mobilités
25 Avenue François Mitterrand
69500 Bron, France
Phone : +33 4 78 65 68 85
https://orcid.org/0000-0001-9245-738X

Raphaël DUMAS, PhD, raphael.dumas@univ-eiffel.fr
LBMC, Univ Eiffel – Cité des Mobilités
25 Avenue François Mitterrand
69500 Bron, France
Phone : +33 4 72 14 23 56

Article submitted as Short Communication / Word Count= 1806

Abstract:
Accuracy of shoulder kinematics predicted by multi-body kinematics optimisation depend on the joint models used.
This study assesses the influence of four different subject-specific gleno-humeral joint models within multi-body kinematics optimisation: a 6-degree-of-freedom joint (i.e. single-body kinematics optimisation), a sphere-on-sphere joint (with two spheres of different radii) and a spherical joint with or without penalised translation. To drive these models, the 3D coordinates of 12 skin markers of 6 subjects performing static arm abduction poses up to 180° were used. The reference data was obtained using biplane X-rays from which 3D bone reconstructions were generated: scapula and humerus were 3D reconstructed by fitting a template model made of geometrical primitives on the two bones' X-rays. Without any motion capture system, the recording of the skin markers was performed at the very same time than the X-rays with radiopaque markers.
The gleno-humeral displacements and angles, and scapula-thoracic angles were computed.
The gleno-humeral sphere-on-sphere joint provided slightly better results than the spherical joint with or without penalised translation, but considerably better gleno-humeral displacements than the 6-DoF joint. Considering that it can easily be personalised from medical images, this sphere-on-sphere model seems promising for shoulder multi-body kinematics optimisation.

Subject-specific model-derived kinematics of the shoulder based on skin markers during arm abduction up to 180° - Assessment of 4 gleno-humeral joint models

Introduction

Shoulder kinematics is generally collected using skin markers and a stereophotogrametric system (Lempereur et al., 2014). However, due to large soft tissue artefact (STA) (Cereatti et al., 2017), a compensation is required to obtain accurate gleno-humeral and scapulo-thoracic kinematics. This compensation relies on a kinematic model of the shoulder and on a multi-body kinematics optimisation (MKO) (Begon et al., 2018) which is sensitive to joint modelling and model parameters (Michaud et al., 2017; Prinold et al., 2013). Specifically, to enable gleno-humeral displacements, apart from a 6-degree-of-freedom (6-DoF) joint, the gleno-humeral joint can be modelled with two spheres of different radii or with a spherical joint with penalised translation (Duprey et al., 2017). These options allow to build subject-specific models, which is key since personalisation improves models' prediction (El Habachi et al., 2013). Personalisation can be performed by functional estimation of the joint centres (Begon et al., 2017; Michaud et al., 2017) or by using 3D bone reconstructions from MRI (Charbonnier et al., 2014; Sarshari et al., 2021).

Few assessments of model-derived shoulder kinematics have been reported: the existing comparative analyses are based on intra-cortical pins (Begon et al., 2017; Naaim et al., 2017) and mono-plane fluoroscopy (Charbonnier et al., 2014). The errors on the gleno-humeral displacements were between 2mm and 4mm when considering penalised translation vs fluoroscopy (Charbonnier et al., 2014). The errors on the gleno-humeral and scapulo-thoracic angles were between 2° and 10° (Begon et al., 2017; Charbonnier et al., 2014; Naaim et al.,

2017). However, no study has evaluated gleno-humeral displacements with a sphere-on-sphere joint model and no study reported accuracy for arm abduction reaching 180°.

Thus, the main objective of this study is to compare the accuracy of 4 models in terms of gleno-humeral and scapulo-thoracic kinematics prediction when using MKO for arm elevation postures up to 180°.

Material and Methods

Arm abduction data

Data from Duprey et al. (2015) was used: biplane X-rays (EOS system) from 6 healthy male participants (30.8±8.5 years, 1.76±0.08m, 69±7.5kg) performing arm abductions at 0°, 45°, 120°, 150°, and 180°. The participants were equipped with 12 radiopaque skin markers enabling to extract their 3D coordinates for each arm abduction within the EOS cabin (were optoelectronic cameras could not fit). One posture (90°) was excluded because all humerus skin markers weren't visible. At the other arm postures, some skin markers were eventually non visible but could be interpolated from the other postures. The 3D geometries of the humerus and scapula were reconstructed from the 0°-posture (anatomical posture) by using a template model made of geometrical primitives and making the primitives fit the bones on the images (for instance, a sphere for the glenoid cavity and the humeral head, a cylinder for the lateral scapula border… (Ohl et al. 2015)). Then, bone models were then matched on the images at higher arm elevations using only rigid translations and rotations (Lagacé et al., 2012) (Figure 1).

Skin markers 3D coordinates and 3D bone reconstructions were recorded simultaneously since they derived from the same images, thus avoiding errors that could be due to calibration of different measurement systems or posture repeatability.

Reference kinematics

The reference kinematics is the gleno-humeral displacements and angles, and scapula-thoracic angles directly extracted from the 3D bone reconstructions. Segment coordinate systems (CS) were defined following the ISB recommendations (Wu et al., 2005) and using bony anatomical landmarks except for the thorax, whose CS was defined using skin markers. The accuracy of the 3D bone reconstruction was estimated at 2.6° for the scapula orientations. The humeral epicondyles weren't always visible, thus the gleno-humeral internal/external rotation hasn't been used.

The reference kinematics (Supplementary Figure 1) was comparable to the literature for arm abduction movement (Dal Maso et al., 2014; Giphart et al., 2013; Ludewig et al., 2009), but advantageously reports results up to 180°.

Comparative assessment

Model-derived kinematics was computed by MKO (Appendix) and compared to reference kinematics. Bland & Altman tests on the 6 subjects and 4 postures were used to compute bias (b, i.e. the mean difference) and the 95% limits of agreement (LoA, i.e. mean difference ± 1.96 standard deviation of the difference). Negative and positive bias respectively indicate under and over estimations. Coefficients of determination (R^2) and root mean square errors (RMSE) were also computed.

Subject-specific model parameters

For the driving constraints used in MKO (Appendix), the position of the skin markers with respect to the bones was defined in the 0°-posture. For the thorax, the skin markers positions in the thorax CS was directly used.

For the kinematic and rigid body constraints used in MKO (Appendix), both radii of the humeral head and glenoid and the scapula length (between acromioclavicular and glenoid centres) were derived from bone reconstructions using virtual palpation (i.e. landmarks detection on the 3D bone reconstructions) and sphere fitting. Clavicle length and humerus length were based on both bone reconstructions (acromioclavicular joint and humeral head centres) and skin markers. Thorax length was based on skin markers only.

Results

Overall, the sphere-on-sphere gleno-humeral joint showed slightly better results than the spherical joint with or without penalised translation, while the 6-DoF joint resulted in apparent dislocations with large displacement errors (Table 1). Results from the 4 gleno-humeral models are in Supplementary Figure 2.

Model-derived gleno-humeral displacements

The accuracy of the predicted gleno-humeral displacements was relatively good with bias about ~2mm and RMSE about 3mm, except for the 6-DoF joint. The bias was negative for each model for the lateral/medial displacement, indicating that this displacement was always systematically underestimated. Considering all goodness-of-fit parameters, single-body kinematics optimisation (6-DoF joint) provided less accurate results (RMSE up to 26mm) for the gleno-humeral displacements than the 3 other studied models.

.

Model-derived gleno-humeral angles

The bias was about -10° for all joint models, indicating a general underestimation of the flexion/extension and adduction/abduction angles. The RMSE was about 16°.

Overall, considering all goodness-of-fit parameters, all of the 3 models used in the MKO and the single-body kinematics optimisation (6-DoF joint) provided comparable results for the gleno-humeral angles.

Model-derived scapulo-thoracic angles

Overall, the scapulothoracic angles deriving from the 4 different models provided closed goodness-of-fit parameters. The bias was about 8° for all joint models for the downward/upward rotation angles. Bias was negative for the posterior/anterior tilt angle (~-3°) indicating a systematic underestimation. The bias was about 3° for the internal/external rotation angle. RMSE were about 10° for each angle and each model.

Considering all goodness-of-fit parameters, single-body kinematics optimisation (6-DoF joint) provided slightly better results for scapulo-thoracic angles.

Discussion

The objective of the present study was to evaluate the accuracy of the gleno-humeral and scapulo-thoracic kinematics obtained by MKO using four subject-specific models during arm abduction up to 180°.

Overall, the gleno-humeral sphere-on-sphere joint provided slightly better results than the spherical joint with or without penalised translation, but considerably better results than the 6-DoF joint (i.e. single-body kinematics optimisation) which resulted in apparent dislocations. Concerning the gleno-humeral displacement, the discrepancies from the reference values seem comparable with the ones deriving from the study of Charbonnier et al. (2014) with a model with penalised translation (RMSE~3mm). This level of errors still appears important relative to the range of motion (< 10mm) and the coefficient of determination was found weak (R^2 =0.16 at best for the sphere-on-sphere joint). To the authors' knowledge, the present study and the one of Charbonnier et al. (2014) are the only ones reporting errors on gleno-humeral displacements and the present study is the first one to quantify the apparent joint dislocation with single-body optimisation (RMSE of 16.0mm to 41.4mm), confirming the interest of multi-body versus single-body kinematics optimisation to predict gleno-humeral displacements.

Concerning the gleno-humeral angles, the level of errors were found higher than previously reported for arm flexion reaching 100° (RMSE<4° with a spherical joint with penalised translation (Charbonnier et al., 2014)) and for different analytical and daily life movements (RMSE=6.1° with a spherical joint and RMSE=10.5° with a 6-DoF joint (Begon et al., 2017)). The level of errors were also found higher than previously reported for the scapulo-thoracic angles (Chu et al., 2012; Karduna et al., 2001; Konda et al., 2018). This may be explained by the fact that larger errors must occur at higher arm elevation (*i.e.* 150° and 180°).

When looking at the inter-model differences, the same tendencies were revealed for open-loop shoulder models (Naaim et al., 2017): RMSEs were found comparable between sphere-on-sphere and spherical joints (7.1° to 9.6° for internal/external rotation and posterior/anterior tilt angles) and maximised with sphere-on-sphere and spherical joints

compared to 6-DoF joint (1.7° to 2.1°). Interestingly, these errors appeared mitigated (2.3° to 4.1°) with a close-loop shoulder model (Naaim et al., 2017).

As for limitations, first, the assessment of the model-derived kinematics was performed on only 6 subjects performing only 4 static postures, due to the difficulty of obtaining reference data (X-rays) for numerous subjects. Furthermore, gleno-humeral internal/external rotation wasn't considered reliable. However, the same concern can be raised with mono-plane fluoroscopy as used by Charbonnier et al. (2014), the perk of bi-plane X-rays being to be minimally invasive. Second, the model-derived kinematics was based on a specific set of skin markers (two clusters of 4 markers placed on the proximal-lateral humerus and on the posterior-lateral acromion) which may maximise the STA. Note that errors in the model-derived kinematics were due to both STA and interpolation of the markers position, especially in postures 120° and 150° where more markers weren't visible. Third, the MKO was based on some, not all, subject-specific model parameters and don't include scapulo-thoracic constraints. Thus, the goodness-of-fit parameters with a complete subject-specific close-loop model of the shoulder remains unknown. Four, the implementation of the spherical joint with penalised translation corresponded to an arbitrary choice of the relative weights between the terms of the objective function. The rationale for this choice was based on the mean amplitude of the gleno-humeral joint displacements (about 1mm to 2mm (Dal Maso et al., 2014; Giphart et al., 2013)) with respect to the STA (10mm to 20mm (Cereatti et al., 2017)). The weights aren't reported in Charbonnier et al. (2014) but the authors stated they were chosen to allow displacements of the same order of magnitude as reported in the literature. Five, the bio-fidelity of the subject-specific kinematic model wasn't evaluated separately from the STA as recommended (Begon et al., 2018) to test the capacity of the model to replicate errorless

skeletal kinematics as performed, for example, for the scapulo-thoracic angles (Naaim et al., 2015; Seth et al., 2016).

To conclude, the sphere-on-sphere joint can be considered as a relevant modelling choice for a gleno-humeral joint with displacements. What is more, the model parameters (radii of humeral head and of glenoid) can be personalised from medical imaging and no arbitrary weighting needs to be defined.

References

Aurbach, M., Spicka, J., Süß, F., Dendorfer, S., 2020. Evaluation of musculoskeletal modelling parameters of the shoulder complex during humeral abduction above 90°. Journal of Biomechanics 106, 109817.

Begon, M., Andersen, M.S., Dumas, R., 2018. Multibody Kinematics Optimization for the Estimation of Upper and Lower Limb Human Joint Kinematics: A Systematized Methodological Review. Journal of Biomechanical Engineering 140.

Begon, M., Bélaise, C., Naaim, A., Lundberg, A., Chèze, L., 2017. Multibody kinematics optimization with marker projection improves the accuracy of the humerus rotational kinematics. Journal of Biomechanics 62, 117-123.

Cereatti, A., Bonci, T., Akbarshahi, M., Aminian, K., Barré, A., Begon, M., Benoit, D.L., Charbonnier, C., Dal Maso, F., Fantozzi, S., Lin, C.-C., Lu, T.-W., Pandy, M.G., Stagni, R., van den Bogert, A.J., Camomilla, V., 2017. Standardization proposal of soft tissue artefact description for data sharing in human motion measurements. Journal of Biomechanics 62, 5-13.

Charbonnier, C., Chagué, S., Kolo, F.C., Chow, J.C.K., Lädermann, A., 2014. A patient-specific measurement technique to model shoulder joint kinematics. Orthopaedics & Traumatology: Surgery & Research 100, 715-719.

Chu, Y., Akins, J., Lovalekar, M., Tashman, S., Lephart, S., Sell, T., 2012. Validation of a video-based motion analysis technique in 3-D dynamic scapular kinematic measurements. Journal of Biomechanics 45, 2462-2466.

Dal Maso, F., Raison, M., Lundberg, A., Arndt, A., Begon, M., 2014. Coupling between 3D displacements and rotations at the glenohumeral joint during dynamic tasks in healthy participants. Clinical Biomechanics 29, 1048-1055.

Duprey, S., Billuart, F., Sah, S., Ohl, X., Robert, T., Skalli, W., Wang, X., 2015. Three-Dimensional Rotations of the Scapula During Arm Abduction: Evaluation of the Acromion Marker Cluster Method in Comparison With a Model-Based Approach Using Biplanar Radiograph Images. Journal of Applied Biomechanics 31, 396-402.

Duprey, S., Naaim, A., Moissenet, F., Begon, M., Chèze, L., 2017. Kinematic models of the upper limb joints for multibody kinematics optimisation: An overview. Journal of Biomechanics 62, 87-94.

El Habachi, A., Duprey, S., Cheze, L., Dumas, R., 2015. A parallel mechanism of the shoulder—application to multi-body optimisation. Multibody System Dynamics 33, 439-451.

El Habachi, A., Duprey, S., Chèze, L., Dumas, R., 2013. Global sensitivity analysis of the kinematics obtained with a multi-body optimisation using a parallel mechanism of the shoulder. Computer Methods in Biomechanics and Biomedical Engineering 16, 61-62.

Giphart, J.E., Brunkhorst, J.P., Horn, N.H., Shelburne, K.B., Torry, M.R., Millett, P.J., 2013. Effect of Plane of Arm Elevation on Glenohumeral Kinematics: A Normative Biplane Fluoroscopy Study. JBJS 95.

Karduna, A.R., McClure, P.W., Michener, L.A., Sennett, B., 2001. Dynamic Measurements of Three-Dimensional Scapular Kinematics: A Validation Study. Journal of Biomechanical Engineering 123, 184-190.

Konda, S., Sahara, W., Sugamoto, K., 2018. Directional bias of soft-tissue artifacts on the acromion during recording of 3D scapular kinematics. Journal of Biomechanics 73, 217-222.

Lagacé, P.-Y., Billuart, F., Ohl, X., Skalli, W., Tétreault, P., de Guise, J., Hagemeister, N., 2012. Analysis of humeral head displacements from sequences of biplanar X-rays: repeatability study and preliminary results in healthy subjects. Computer Methods in Biomechanics and Biomedical Engineering 15, 221-229.

Lempereur, M., Brochard, S., Leboeuf, F., Rémy-Néris, O., 2014. Validity and reliability of 3D marker based scapular motion analysis: A systematic review. Journal of Biomechanics 47, 2219-2230.

Ludewig, P.M., Phadke, V., Braman, J.P., Hassett, D.R., Cieminski, C.J., LaPrade, R.F., 2009. Motion of the Shoulder Complex During Multiplanar Humeral Elevation. JBJS 91.

Michaud, B., Duprey, S., Begon, M., 2017. Scapular kinematic reconstruction – segmental optimization, multibody optimization with open-loop or closed-loop chains: which one should be preferred? International Biomechanics 4, 86-94.
Naaim, A., Moissenet, F., Dumas, R., Begon, M., Chèze, L., 2015. Comparison and validation of five scapulothoracic models for correcting soft tissue artefact through multibody optimisation. Computer Methods in Biomechanics and Biomedical Engineering 18, 2014-2015.
Naaim, A., Moissenet, F., Duprey, S., Begon, M., Chèze, L., 2017. Effect of various upper limb multibody models on soft tissue artefact correction: A case study. Journal of Biomechanics 62, 102-109.
Prinold, J.A.I., Masjedi, M., Johnson, G.R., Bull, A.M.J., 2013. Musculoskeletal shoulder models: A technical review and proposals for research foci. Proceedings of the Institution of Mechanical Engineers, Part H: Journal of Engineering in Medicine 227, 1041-1057.
Quental, C., Folgado, J., Ambrósio, J., Monteiro, J., 2016. A new shoulder model with a biologically inspired glenohumeral joint. Medical Engineering & Physics 38, 969-977.
Sarshari, E., Farron, A., Terrier, A., Pioletti, D., Mullhaupt, P., 2017. A simulation framework for humeral head translations. Medical Engineering & Physics 49, 140-147.
Sarshari, E., Mancuso, M., Terrier, A., Farron, A., Mullhaupt, P., Pioletti, D., 2021. Feasibility of an alternative method to estimate glenohumeral joint center from videogrammetry measurements and CT/MRI of patients. Computer Methods in Biomechanics and Biomedical Engineering 24, 33-42.
Šenk, M., Chèze, L., 2006. Rotation sequence as an important factor in shoulder kinematics. Clinical Biomechanics 21, S3-S8.
Seth, A., Matias, R., Veloso, A.P., Delp, S.L., 2016. A Biomechanical Model of the Scapulothoracic Joint to Accurately Capture Scapular Kinematics during Shoulder Movements. PLOS ONE 11, e0141028.
Wu, G., van der Helm, F.C.T., Veeger, H.E.J., Makhsous, M., Van Roy, P., Anglin, C., Nagels, J., Karduna, A.R., McQuade, K., Wang, X., Werner, F.W., Buchholz, B., 2005. ISB recommendation on definitions of joint coordinate systems of various joints for the reporting of human joint motion—Part II: shoulder, elbow, wrist and hand. Journal of Biomechanics 38, 981-992.

Appendix

The positions of the humerus, scapula, and thorax were estimated from the skin markers using a MKO based on natural coordinates **Q** (El Habachi et al. 2013) :

$$\mathbf{Q}^* = \arg\min_{\mathbf{Q}} \left(\frac{1}{2} \left(\mathbf{\Phi}^m \right)^T \mathbf{W} \left(\mathbf{\Phi}^m \right) \right)$$
$$\text{subject to } \begin{cases} \mathbf{\Phi}^k = \mathbf{0} \\ \mathbf{\Phi}^r = \mathbf{0} \end{cases},$$

where the driving constraints $\mathbf{\Phi}^m$, kinematic constraints $\mathbf{\Phi}^k$, and rigid body constraints $\mathbf{\Phi}^r$ were defined according to the 3D bone reconstructions performed in the anatomical standing posture (see section below). The driving constraints corresponded to skin markers coordinates. In the optimisation, all marker weights were set to 1 (**W** is identity matrix). The shoulder model was an open loop without scapulo-thoracic constraints. The kinematic constraints corresponded to a constant clavicle length between sterno-clavicular and acromio-clavicular joints and to (i) a sphere-on-sphere joint with two spheres of different radii, (ii) a spherical joint, (iii) a spherical joint with penalised translation, or (iv) a 6-DoF joint. In the last case, the constant clavicle length was also released leading to a special case of MKO: single-body kinematics optimisation where humerus, scapula, and thorax were processed separately. In case of penalised translation, the gleno-humeral displacements were all weighted 5 so that the penalty terms (sum of squared displacements $\mathbf{\Phi}^{k_1}$) vs the marker tracking term was about 1 vs 200:

$$\mathbf{Q}^* = \arg\min_{\mathbf{Q}} \left(\frac{1}{2} \left(\begin{matrix} \mathbf{\Phi}^m \\ \mathbf{\Phi}^{k_1} \end{matrix} \right)^T \mathbf{W} \left(\begin{matrix} \mathbf{\Phi}^m \\ \mathbf{\Phi}^{k_1} \end{matrix} \right) \right)$$
$$\text{subject to } \begin{cases} \mathbf{\Phi}^{k_2} = \mathbf{0} \\ \mathbf{\Phi}^r = \mathbf{0} \end{cases}.$$

The rigid body constraints corresponded to constant angles and lengths dealing with the two points positions and two axes orientations as defined in the natural coordinates **Q** (El Habachi et al. 2015).

Model-derived kinematics was computed from the optimised coordinates **Q***. The gleno-humeral displacements were expressed about scapula axes. The gleno-humeral angles were computed using a XZY sequence of rotations (Senk and Chèze 2006) and the scapulo-thoracic angles using a YXZ sequence (Wu et al. 2005).

References

El Habachi A, Duprey S, Cheze L, Dumas R. 2013. Global sensitivity analysis of the kinematics obtained with a multi-body optimisation using a parallel mechanism of the shoulder. In: Comput Methods Biomech Biomed Engin [Internet]. Vol. 16. Marseille, France; [accessed 2016 Apr 25]; p. 61–62. http://www.tandfonline.com/doi/full/10.1080/10255842.2013.815907

El Habachi A, Duprey S, Cheze L, Dumas R. 2015. A parallel mechanism of the shoulder—application to multi-body optimisation. Multibody Syst Dyn. 33(4):439–451. https://doi.org/10.1007/s11044-014-9418-7

Senk M, Chèze L. 2006. Rotation sequence as an important factor in shoulder kinematics. Clin Biomech. 21:S3–S8. https://doi.org/10.1016/j.clinbiomech.2005.09.007

Wu G, van der Helm FCT, (DirkJan) Veeger HEJ, Makhsous M, Van Roy P, Anglin C, Nagels J, Karduna AR, McQuade K, Wang X, et al. 2005. ISB recommendation on definitions of joint coordinate systems of various joints for the reporting of human joint motion—Part II: shoulder, elbow, wrist and hand. J Biomech. 38(5):981–992. https://doi.org/10.1016/j.jbiomech.2004.05.042

Figure captions

Figure 1: Experimental set-up at 120° of arm posture (left) and 3D data for all arm postures (right): thorax markers (orange), clusters of markers on the acromion (red) and on the humerus (blue), 3D bone reconstructions (grey), thorax, scapula, and humerus model segments (black). Reader can refer to the online version of the article for a colored version of the figure.

Table 1: Goodness-of-fit parameters (b, LoA, R^2, and RMSE) for model-derived gleno-humeral and scapulo-thoracic kinematics

FIG. 1.

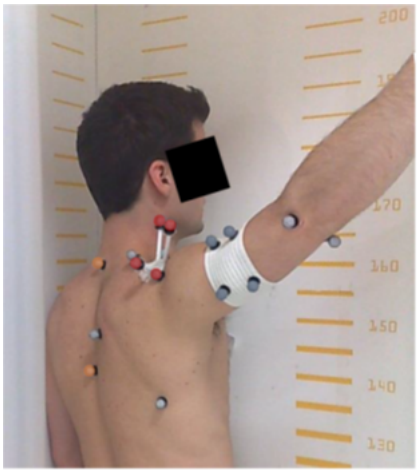

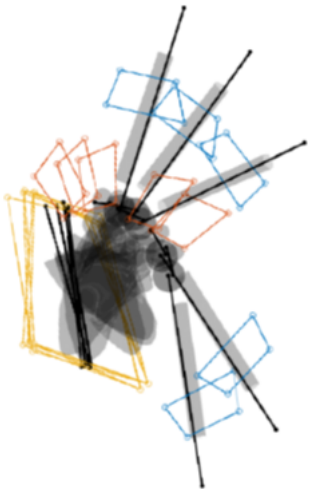

Table 1

		Sphere-on-Sphere	Spherical	Penalised translation	6 DoF
Gleno-humeral anterior/posterior displacement	b	2.8	0.8	1.7	5.5
	LoA	7.2	6.0	5.7	23.0
	R^2	0.00	N/A	0.10	0.02
	RMSE	4.5	3.1	3.3	12.6
Gleno-humeral proximal/distal displacement	b	0.6	2.6	1.3	-1.4
	LoA	7.2	5.0	5.9	27.8
	R^2	0.12	N/A	0.01	0.15
	RMSE	3.6	3.6	3.2	13.9
Gleno-humeral lateral/medial displacement	b	-1.9	-1.4	-1.5	-4.8
	LoA	6.5	3.6	3.5	52.3
	R2	0.15	N/A	0.08	0.04
	RMSE	3.7	2.3	2.3	26.4
Gleno-humeral adduction/abduction	b	-11.0	-11.6	-10.1	-12.1
	LoA	27.7	24.8	27.9	44.4
	R^2	0.86	0.89	0.85	0.67
	RMSE	17.6	16.9	17.1	25.1
Gleno-humeral flexion/extension	b	-7.1	-8.0	-8.3	-6.3
	LoA	23.9	23.3	23.9	22.4
	R^2	0.56	0.58	0.59	0.64
	RMSE	13.8	14.0	14.5	12.8
Scapulo-thoracic internal/external rotation	b	3.3	5.9	2.1	3.1
	LoA	14.8	15.1	18.6	17.6
	R^2	0.13	0.16	0.02	0.14
	RMSE	8.1	9.5	9.5	9.3
Scapulo-thoracic downward/upward rotation	b	9.1	9.9	8.7	6.8
	LoA	15.3	15.3	15.5	14.9
	R^2	0.84	0.84	0.84	0.84
	RMSE	11.9	12.4	11.6	10.0
Scapulo-thoracic posterior/anterior tilt	b	-3.9	-4.7	-1.4	-4.3
	LoA	15.4	14.4	20.0	12.9
	R^2	0.48	0.50	0.37	0.61
	RMSE	8.6	8.6	10.0	7.7